



# *In vivo* real-time visualization of tissue blood flow and angiogenesis using Ag<sub>2</sub>S quantum dots in the NIR-II window



Chunyan Li, Yejun Zhang, Mao Wang, Yan Zhang, Guangcun Chen, Lun Li, Dongmin Wu, Qiangbin Wang\*

Suzhou Key Laboratory of Nanomedical Characterization, Division of Nanobiomedicine and i-Lab, Suzhou Institute of Nano-Tech and Nano-Bionics, Chinese Academy of Sciences, Suzhou 215123, China

## ARTICLE INFO

### Article history:

Received 8 August 2013

Accepted 1 October 2013

Available online 15 October 2013

### Keywords:

Ag<sub>2</sub>S Quantum dots

*In vivo* imaging

Fluorescence

Second near-infrared window

## ABSTRACT

Improving the tissue penetration depth and spatial resolution of fluorescence-based optical nanoprobes remains a grand challenge for their practical applications in *in vivo* imaging, due to the scattering and absorption and endogenous autofluorescence of living tissues. Here, we present that Ag<sub>2</sub>S quantum dots (QDs), containing no toxic ions, exhibiting long circulation time and high stability, act as a new kind of fluorescent probes in the second near-infrared window (NIR-II, 1000–1350 nm) which enable *in vivo* monitoring of lymphatic drainage and vascular networks with deep tissue penetration and high spatial and temporal resolution. In addition, NIR-II fluorescence imaging with Ag<sub>2</sub>S QDs provide ultrahigh spatial resolution (~40 μm) that permits us to track angiogenesis mediated by a tiny tumor (2–3 mm in diameter) *in vivo*. Our results indicate that Ag<sub>2</sub>S QDs are promising NIR-II fluorescent nanoprobes that could be useful in surgical treatments such as sentinel lymph node (SLN) dissection as well in assessment of blood supply in tissues and organs and screening of anti-angiogenic drugs.

© 2013 Elsevier Ltd. All rights reserved.

## 1. Introduction

The circulatory system, consisting of blood vessels and lymphatic drainage systems, is vital to life and participates in many pathological processes, including tumorigenesis and metastasis. *In vivo* real-time visualization of the circulatory system has great potential to improve our understanding of circulatory system-related physiological and pathological processes and to advance clinical diagnostics and therapy [1,2]. Current methods for assessing vasculature and lymphatic drainage *in vivo*, such as microscopic computed tomography (micro-CT), magnetic resonance imaging (MRI), and nuclear medicine (positron emission tomography [PET] and single photon emission computed tomography [SPECT]), have the advantage of unlimited penetration depth, but they also have inherent problems. For instance, CT and MRI often require high doses of contrast [3–6]. High-energy photon imaging, such as PET and SPECT, has high sensitivity but requires radioactive tracers that can put patients and operators at risk [4,5]. In addition, these techniques are not ideal for visualizing real-time dynamics, due to their long image acquisition and post-processing time.

Intravital fluorescence-based optical imaging has inherent advantages owing to its high sensitivity, fast feedback, multiplexing, and absence of ionizing radiation. Several fluorescence imaging agents with emission <1000 nm, such as dextrans [7], lectins [8], antibodies [9], and quantum dots (QDs) [10,11], have been used for imaging microvasculature and lymph nodes. However, minimal penetration depth with low feature fidelity has largely limited their further clinical applications. Fluorescence imaging in the second near-infrared region (NIR-II, 1000–1350 nm) is more desirable than visible (450–700 nm) and traditional NIR-I imaging (700–950 nm) owing to greatly reduced photon absorption and scattering by tissues, as well as negligible tissue autofluorescence, which promises high-fidelity imaging of deeper tissues and organs [12–15]. Single-walled carbon nanotubes (SWNTs) have attracted intense attention in *in vivo* imaging in the last five years due to their appealing NIR-II emission [13,16–24]. In particular, Dai group has made significant breakthroughs in noninvasively obtaining the *in vivo* information by using SWNTs as the NIR-II fluorescent probe [13,16–23]. However, SWNTs are suffering from their low quantum yield (QY) and the difficulty in clearance from the body due to their large length in hundreds of nanometers [16–18].

Unlike SWNTs, NIR-emitting QDs can be finely tuned in size and shape to modulate pharmacokinetics and tissue distribution [25], and they exhibit outstanding tunability in their optical properties,

\* Corresponding author.

E-mail address: [qbwang2008@sinano.ac.cn](mailto:qbwang2008@sinano.ac.cn) (Q. Wang).

such as CdHgTe [26], PbSe [27], PbS [28], etc. Recently, Ag<sub>2</sub>S QDs with bright NIR-II emission, high photostability, and decent biocompatibility have been demonstrated as a promising candidate for *in vivo* dynamic imaging of deep inner organs and tumor in mice [29–33]. Herein, to help improving our understanding of circulatory system-related physiological and pathological processes and advancing clinical diagnostics and therapy, we explore the *in vivo* dynamic imaging of circulatory system by using Ag<sub>2</sub>S QDs, including lymphatic monitoring, blood flow, and angiogenesis mediated by subcutaneous xenograft tumors in mice.

## 2. Materials and methods

### 2.1. Synthesis of PEGylated Ag<sub>2</sub>S QDs

Ag<sub>2</sub>S QDs were first synthesized in organic phase according to previously reported methods [31,32]. Briefly, a mixture of (C<sub>2</sub>H<sub>5</sub>)<sub>2</sub>NCS<sub>2</sub>Ag (0.1 mmol) and 10 g of 1-dodecanethiol (DT) was added into a three-necked flask (100 mL) at room temperature. The oxygen was removed from the flask by vacuuming for 5 min under vigorous magnetic stirring. Then, the solution was heated to 210 °C at a heating rate of 15 °C/min and kept at 210 °C for 1 h under N<sub>2</sub> atmosphere. After cooling to room temperature naturally, 50 mL of ethanol was added into the solution, and the resultant mixture was separated through centrifugation with a centrifugal force of 6729 g for 20 min, then the precipitates were collected. The surface of the as-prepared Ag<sub>2</sub>S QDs about 5.6 nm in diameter is coated with hydrophobic DT. To make Ag<sub>2</sub>S QDs hydrophilic, the QDs were then coated with a surfactant dihydrochloric acid (DHHLA) to displace DT by ligand exchange. A mixture of as-prepared hydrophobic Ag<sub>2</sub>S sample (0.05 mmol), cyclohexane (15 mL), ethanol (15 mL) and DHHLA (0.15 g) were stirred at room temperature for 48 h. The product was isolated through centrifugation with a centrifugal force of 26,916 g for 20 min, and then washed with deionized water and re-dispersed in deionized water. Then 24 mg of six-armed PEG (10 KD) and 120 μL of EDC/NHS (20 mg/mL) were added into the DHHLA-Ag<sub>2</sub>S solution. After sonication for 30 min, another 360 μL of EDC/NHS (20 mg/mL) were added, and stirred for 8 h. The product was then isolated by centrifugation with a centrifugal force of 26,916 g for 20 min and washed with 1 × PBS buffer three times, and then re-dispersed in 1 × PBS buffer.

### 2.2. Characterizations

#### 2.2.1. Transmission electron microscopy (TEM)

The morphologies of as-prepared Ag<sub>2</sub>S QDs were examined by a Tecnai G2 F20 S-Twin transmission electron microscopy (TEM, FEI, USA) operated at 200 kV.

#### 2.2.2. UV–vis–NIR absorption measurements

The UV–vis–NIR absorption spectrum of PEGylated Ag<sub>2</sub>S QDs was measured by a Perkin–Elmer Lambda 25 UV–vis spectrometer, background-corrected for contribution from water. The measured range was from 400 nm to 900 nm.

#### 2.2.3. NIR fluorescence spectroscopy of PEGylated Ag<sub>2</sub>S QDs

The NIR fluorescence spectrum was measured using an Applied Nano-Fluorescence spectrometer (USA) at room temperature with an excitation laser source of 658 nm. The collected range was from 900 nm to 1600 nm.

#### 2.2.4. Stability of PEGylated Ag<sub>2</sub>S QDs

To determine the colloidal stability of PEGylated Ag<sub>2</sub>S QDs under various aqueous and buffer conditions over time, samples were measured using a Malvern Nanosizer. Samples were loaded in 2 mL cuvettes and run at 10% power (to prevent saturated counts). Measurements were collected at 10 s intervals. Each sample was run 15 times.

Fluorescent stability of PEGylated Ag<sub>2</sub>S QDs (1 μM, 0.375 mg/mL) was measured by analysis of mean fluorescent pixel intensity after 120 min of irradiation with an 808 nm laser diode at 123.8 mW/cm<sup>2</sup>.

### 2.3. *In vivo* fluorescence imaging of mice

Visible and NIR-I fluorescence imaging were carried out by using Maestro *in vivo* imaging system (CRI Inc, USA) under excitation at 455 nm and 704 nm and collection at 630 ± 50 nm and 830 ± 50 nm, respectively. NIR-II fluorescence imaging, including lymphatic imaging, blood pool imaging, and tumor angiogenesis imaging, was performed with a 640 × 512 pixel two-dimensional InGaAs/SWIR camera (Photonic Science, UK) equipped with an 880-nm long-pass filter and an 1100-nm long-pass filter (Daheng Optics and Fine Mechanics Co., Ltd, China). A near-infrared lens pair SWIR-35 (Navitar, US) was used to focus the image onto the detector. The excitation light was provided by an 808-nm diode laser (Starway Laser Inc., China). The excitation power density at the imaging plane was 45 mW/cm<sup>2</sup>.

### 2.4. Video-rate imaging in the NIR-II window

For video-rate imaging, the same home-built imaging system was employed for imaging in NIR-II region. The excitation light was provided by an 808-nm diode laser

(Starway Laser Inc., China). The excitation power density at the imaging plane was 45 mW/cm<sup>2</sup>. The emitted light from the mouse was filtered through a 880-nm long-pass filter and a 1100-nm long-pass filter (Daheng Optics and Fine Mechanics Co., Ltd, China) so that the intensity of each pixel in the InGaAs/SWIR two-dimensional array represented light in the 1.1–1.7 μm range. A near-infrared lens pair SWIR-35 (Navitar, US) was used to focus the image onto the detector. InGaAs camera was set to expose continuously, and NIR-II fluorescence images were acquired with LabVIEW software. The exposure time for all images shown in the videos was 50 ms.

### 2.5. Dynamic contrast-enhanced imaging based on PCA

Dynamic contrast-enhanced images were obtained according to the previous method by the Hillman group and Dai group [13,34]. For blood pool imaging, the first 300 consecutive frames (15 s) immediately after injection were loaded into an array using MATLAB software, and the built-in princomp function was used to perform PCA. For positive images, the positive pixels for second, third, fourth, and fifth principal components were assigned green, blue, yellow, and cyan respectively, and overlaid. For negative images, the negative pixels for second, third, fourth, and fifth principal components were assigned green, blue, yellow, and cyan respectively, and overlaid. For combined images, the absolute value of the principal component scores was used.

### 2.6. Histology

Animals were euthanized with 10% chloral hydrate (20 μL) followed by cervical dislocation. After the skin had been removed, fluorescent imaging was taken to improve the visualization of the positions of the fluorescent lymph nodes. OCT-embedded tissue was cryo-sectioned at 6 μm onto Superfrost Plus slides. Tissue sample was further stained with hematoxylin and eosin and subsequently imaged via light microscopy (Olympus, CKX31/41).

## 3. Results and discussion

### 3.1. PEGylated Ag<sub>2</sub>S QDs

PEGylated Ag<sub>2</sub>S QDs with NIR-II fluorescent emission were synthesized according to previously reported methods [31,32]. A typical transmission electron microscopy (TEM) image (Fig. 1a) showed that Ag<sub>2</sub>S QDs were nearly monodispersed with an average diameter of 5.6 nm. The QDs with a quantum yield of ~16% exhibited peak emission at 1200 nm and presented typical broad band absorption properties (Fig. 1b). Because of the surface coating of PEG polymer, these PEGylated Ag<sub>2</sub>S QDs displayed high colloidal stability in different buffer solutions (Fig. 1c and d, Supplementary Fig. S1). Photobleaching experiment showed that even after 120 min of irradiation with an 808 nm laser diode at 123.8 mW/cm<sup>2</sup>, the Ag<sub>2</sub>S QDs retained about 70% of their initial NIR-II photoluminescence without significant further decay, while the reference of a small molecule fluorescence dye indocyanine green (ICG) (NIR-I, 835 nm) showed poor photostability (Fig. 1e). Moreover, in order to determine the tissue scattering of NIR-II Ag<sub>2</sub>S QDs, a standard tissue phantom procedure using commercially available intralipid solution was further performed. Capillaries that contained a solution of ICG or Ag<sub>2</sub>S QDs in PBS were immersed in the liquid at a depth of 6 mm. Fluorescence images were captured while increasing the intralipid concentration from 0 to 1.5%, which approaches the tissue content in body. As shown in Fig. 1f and g and Supplementary Fig. S2, the image clarity gradually decreased, due to the enhanced scattering at higher concentration of intralipid. However, compared with ICG (NIR-I emission peak at 835 nm), Ag<sub>2</sub>S QDs (NIR-II emission peak at 1200 nm) maintained higher image fidelity and integrity that were attributable to minimized scattering in the NIR-II window, consistent with the findings of previous reports [13,15]. A quantitative analysis of tissue penetration of PEGylated Ag<sub>2</sub>S QDs (0.1 mg/mL) in a tissue phantom model gives high penetration depth (>1.1 cm) (Supplementary Fig. S3).

### 3.2. *In vivo* imaging of the lymphatic system

Identification and dissection of lymphatic system in cancer patients, including lymphatic vessels and lymph nodes, are of high

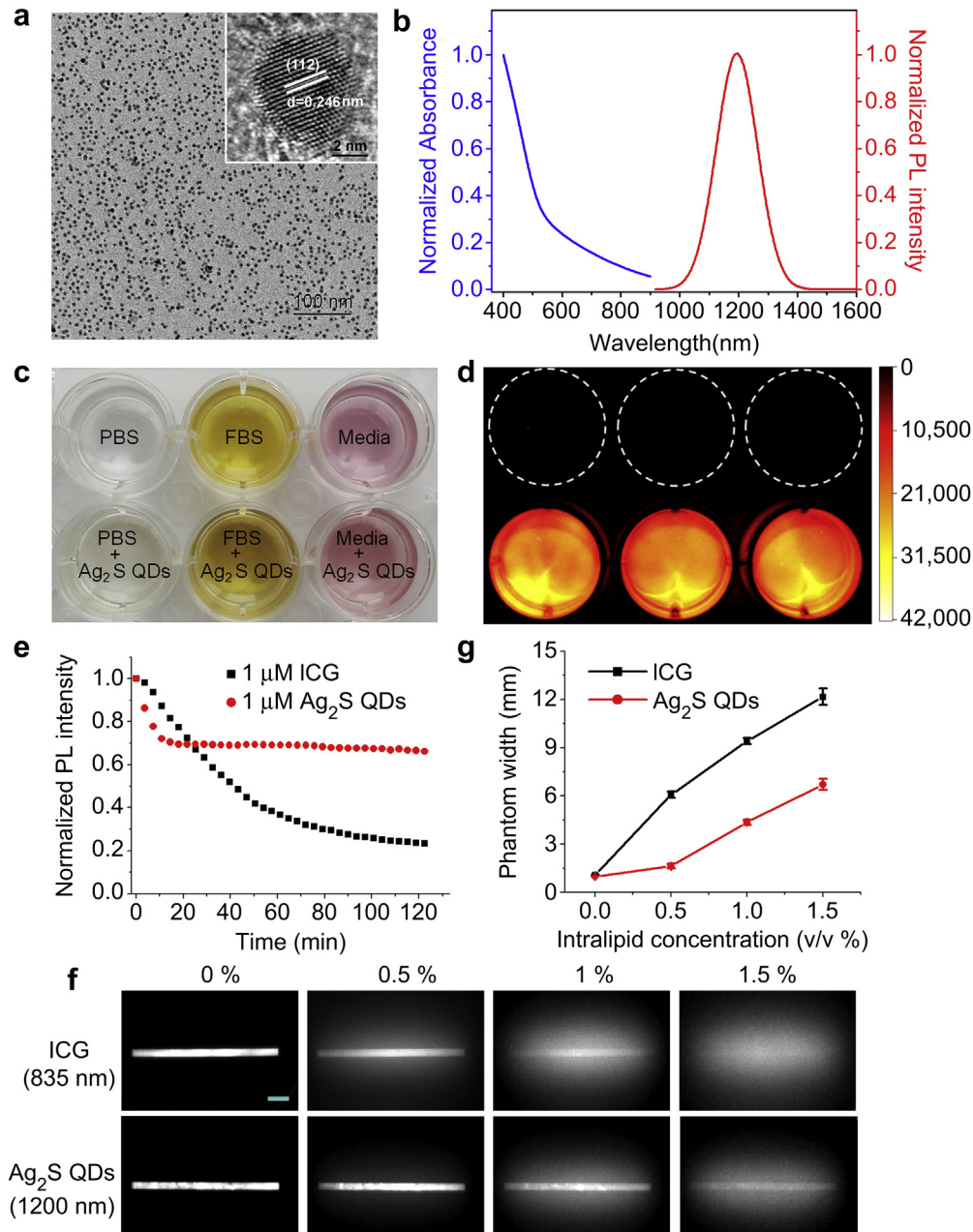


**Fig. 1.** Characterization of PEGylated  $\text{Ag}_2\text{S}$  QDs. (a) TEM and HR-TEM (inset) image of monodispersed PEGylated  $\text{Ag}_2\text{S}$  QDs. (b) Absorbance and photoluminescence spectra of PEGylated  $\text{Ag}_2\text{S}$  QDs. (c) Dispersion of PEGylated  $\text{Ag}_2\text{S}$  QDs at a concentration of 0.1 mg/mL in PBS (left), fetal bovine serum (FBS) (middle), and cell culture media (RPMI 1640) (right) at room temperature. (d) NIR-II fluorescent images of the PEGylated  $\text{Ag}_2\text{S}$  QDs solutions in (c). (e) Photostability of PEGylated  $\text{Ag}_2\text{S}$  QDs and ICG after 120 min of irradiation with an 808 nm laser diode at 123.8 mW/cm<sup>2</sup>. (f) Tissue phantom study of  $\text{Ag}_2\text{S}$  QDs and ICG. Fluorescence images of ICG (NIR-I, 835 nm) and  $\text{Ag}_2\text{S}$  QDs (NIR-II, 1200 nm) immersed in different concentration of intralipid solutions at a depth of 6 mm with a 808 nm excitation (the power density of 90.2 mW/cm<sup>2</sup>). Scale bar represents 0.5 cm. (g) Phantom width of  $\text{Ag}_2\text{S}$  QDs and ICG capillary images corresponding to (f), showing a narrower feature width of NIR II-emitting  $\text{Ag}_2\text{S}$  QDs in comparison with the NIR I-emitting ICG.

importance and have revolutionized cancer surgery. We explored the use of  $\text{Ag}_2\text{S}$  QDs in lymphography. PEGylated  $\text{Ag}_2\text{S}$  QDs were administered by subcutaneous injection (1 mg/mL, 50  $\mu\text{L}$ ) in footpads of nude mice ( $n = 3$ ). The  $\text{Ag}_2\text{S}$  QDs, which were recorded *in situ* using an InGaAs CCD camera under an excitation of 808 nm with an illumination density of 45 mW/cm<sup>2</sup>, entered the lymphatics and migrated within minutes to the popliteal and lumbar lymph nodes (Fig. 2, Supplementary Fig. S4, and Supplementary Movie S1). Lymphatic vessels that diverged from the injection site and then coalesced at the sentinel lymph node (SLN) were also unambiguously identified. After reinjection of the same site with the lymphatic counterstain methylene blue (MB), the MB was

perfectly colocalized with the fluorescence of the  $\text{Ag}_2\text{S}$  QDs (Supplementary Fig. S5a–c). This observation was confirmed by histological analysis (Supplementary Fig. S5d and e). In order to distinguish the *in vivo* fluorescence imaging in NIR-I and NIR-II window, same amount of ICG and PEGylated  $\text{Ag}_2\text{S}$  QDs were injected in the left and right footpad of a mouse, respectively. As shown in Fig. 2b and c, the lymph nodes and vessel anatomy observed with  $\text{Ag}_2\text{S}$  QDs as an imaging agent are much sharper in comparison with those of ICG due to the less scattering and absorbance of photons in NIR-II window. Ideal penetration depth with high feature fidelity in the NIR-II window indicates the potential of  $\text{Ag}_2\text{S}$  QDs to provide direct visual guidance to surgeons

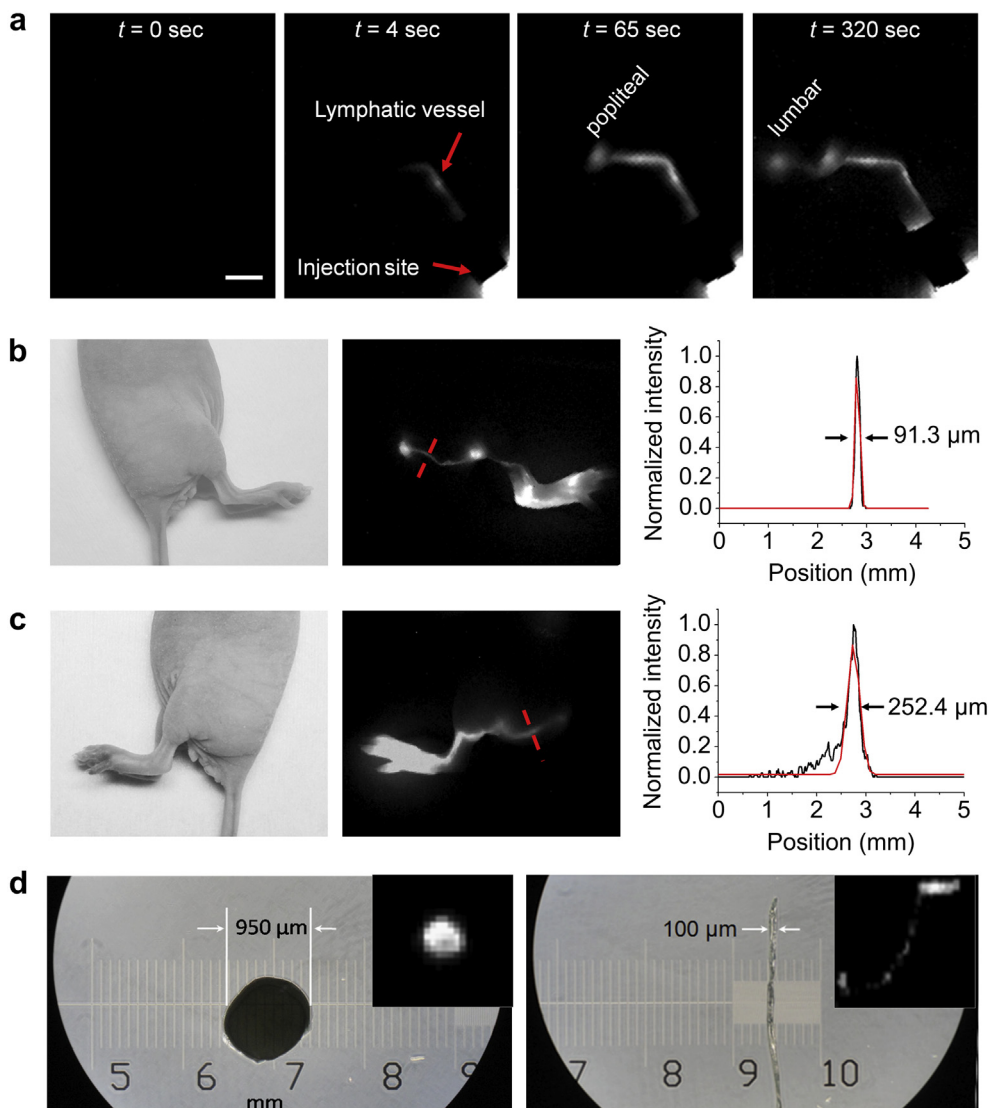


**Fig. 2.** *In vivo* imaging of the lymphatic system with ICG (835 nm, NIR-I) and  $\text{Ag}_2\text{S}$  QDs (1200 nm, NIR-II). (a) Time-course NIR-II fluorescence imaging of lymphatic drainage in the nude mouse after subcutaneous injection with  $\text{Ag}_2\text{S}$  QDs (1 mg/mL, 50  $\mu\text{L}$ ) into the footpad. Images were acquired after 0, 4, 65, and 320 s, respectively. Scale bar represents 2 mm. (b) Bright field (left) and fluorescence (middle) images of live mice by subcutaneous injection of PEGylated  $\text{Ag}_2\text{S}$  QDs (1 mg/mL, 50  $\mu\text{L}$ ) into right footpad. Cross-sectional fluorescence intensity profiles (right) along red-dashed bars of a mouse injected with the QDs. Gaussian fits to the profiles are shown in red-dashed curves. (c) Bright field (left) and fluorescence (middle) images of live mice by subcutaneous injection of ICG (1 mg/mL, 50  $\mu\text{L}$ ) into left footpad. Cross-sectional fluorescence intensity profiles (right) along red-dashed bars of a mouse injected with ICG. Gaussian fits to the profiles are shown in red-dashed curves. (d) Size of the lymph node (left) and lymphatic vessel (right) extracted from the mouse under NIR-II fluorescence guidance after injection with  $\text{Ag}_2\text{S}$  QDs. Inset, fluorescent images of the lymph node and lymphatic vessel. (For interpretation of the references to color in this figure legend, the reader is referred to the web version of this article.)

throughout the entire SLN mapping procedure and minimize inaccuracies in incision and dissection. Indeed, SLN and lymphatic vessels with diameters of  $\sim 950 \mu\text{m}$  and  $\sim 100 \mu\text{m}$ , respectively, were precisely removed under NIR-II fluorescence guidance after administration of PEGylated  $\text{Ag}_2\text{S}$  QDs (Fig. 2d).

Supplementary video related to this article can be found at <http://dx.doi.org/10.1016/j.biomaterials.2013.10.010>.

### 3.3. Blood pool imaging

Angiography is another important mode of circulatory system imaging and is of great interest in cancer diagnosis and therapy. We evaluated the feasibility of PEGylated  $\text{Ag}_2\text{S}$  QDs as a probe for NIR-II imaging of blood circulation. A 200  $\mu\text{L}$  suspension of PEGylated  $\text{Ag}_2\text{S}$  QDs (1 mg/mL in PBS) was injected intravenously into a mouse. Intense fluorescence was detected within a few minutes

after injection under an excitation of 808 nm with an illumination density of 45  $\text{mW}/\text{cm}^2$ , and the whole vascular network of the mouse was clearly visualized (Fig. 3). Video-rate fluorescent images based on the intrinsic NIR-II fluorescence of  $\text{Ag}_2\text{S}$  QDs were obtained continuously immediately after injection to track the circulation of QDs in real time up to 76.2 s post-injection (Fig. 3a). These images showed the QDs returning to the heart after intravenous injection and then entering the pulmonary circulation before being pumped into the whole body. The QDs were preferentially associated with the lumen peripheries of vessels and were distributed throughout larger vessels into smaller vessels (Fig. 3 and Supplementary Movie S2). Moreover, the minimal autofluorescence and low absorption and scattering of NIR-II emission afforded maximal penetration depth for deep tissue imaging with high feature fidelity, which facilitated the imaging of deeper organs such as the heart, lungs, liver, and spleen. High-order branches of blood vessels were

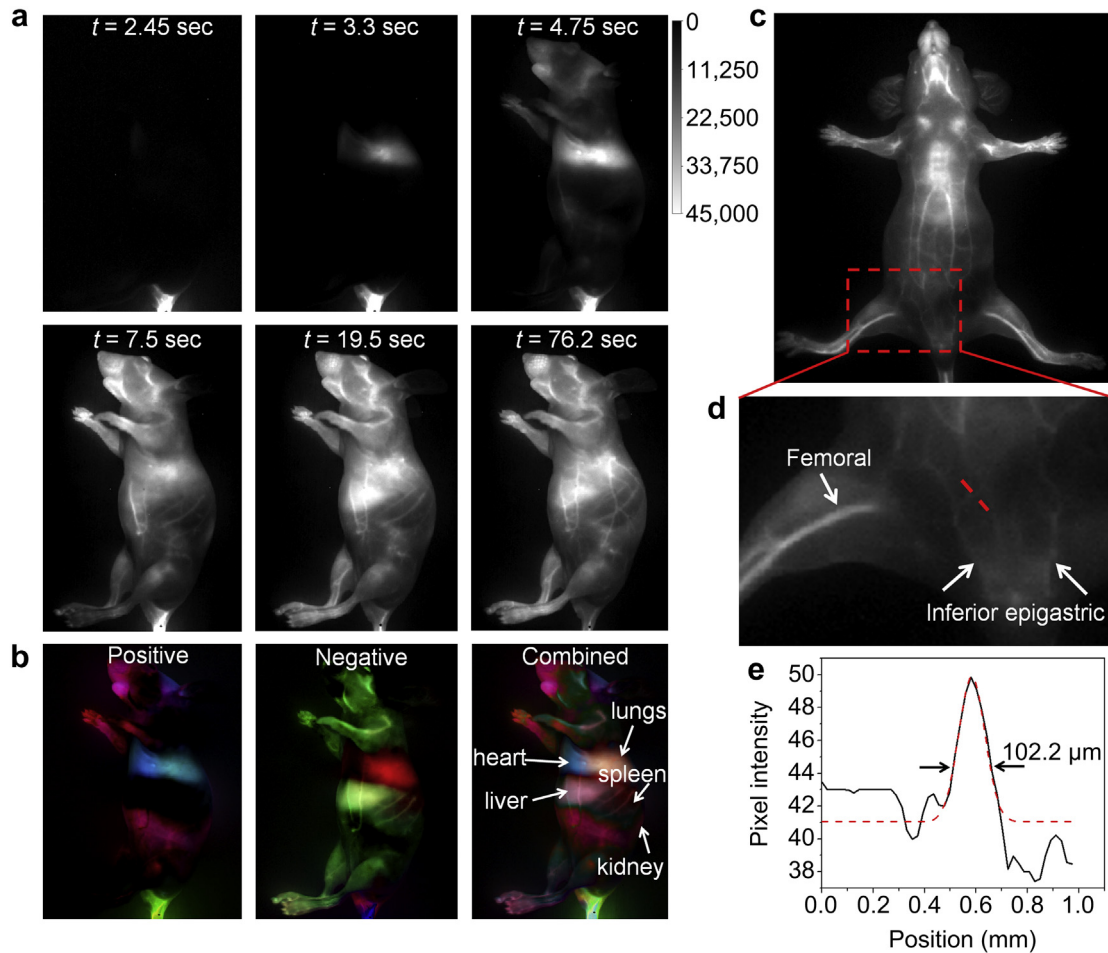


**Fig. 3.** Blood pool imaging of the nude mouse. (a) Time-course NIR-II fluorescence images of blood flow in the nude mouse after injection of PEGylated  $\text{Ag}_2\text{S}$  QDs (1 mg/mL, 200  $\mu\text{L}$ ). (b) Dynamic contrast-enhanced images with PEGylated  $\text{Ag}_2\text{S}$  QDs based on PCA analysis. PCA images were obtained over the first 15 s (300 frames) immediately after injection. Deep organs such as heart, lungs, liver, spleen, and kidney were observed. (c) Intravital NIR-II fluorescence image of the nude mouse in supine position. (d) Amplified fluorescent image of vasculature in the nude mouse. (e) A cross-sectional intensity profile measured along the red-dashed line in (d) with its peak fitted to Gaussian functions. The PL signal from the  $\text{Ag}_2\text{S}$  QDs is easily distinguishable from the endogenous autofluorescence without any image processing. (For interpretation of the references to color in this figure legend, the reader is referred to the web version of this article.)

well defined with high spatial resolution, even a small vessel with a diameter of  $\sim 102 \mu\text{m}$  was unambiguously observed without using a zoom-in lens. To obtain further physiological and anatomical information of the mouse, principal component analysis (PCA) was applied to a time series of fluorescence imaging in the first 15 s (300 frames) immediately after injection. Major tissues and organs were precisely delineated and identified based on their circulations (Fig. 3b). Notably, compared with ICG which is removed from the circulation to bile juice exclusively by the liver in a short time (Supplementary Fig. S6), PEGylated  $\text{Ag}_2\text{S}$  QDs with decent blood circulation half-time of 4.1 h (Supplementary Fig. S7) remain bright and are localized in the body for more than 9 h (Supplementary Fig. S8). These findings suggest that PEGylated  $\text{Ag}_2\text{S}$  QDs may be very promising in *in vivo* real-time visualization of vascular structures and in vascular-related disease imaging, especially for assessment of blood supply in tissues and organs.

Supplementary video related to this article can be found at <http://dx.doi.org/10.1016/j.biomaterials.2013.10.010>.

#### 3.4. *In vivo* imaging of angiogenesis

The growth of new blood vessels from pre-existing vasculature, namely, angiogenesis, is essential for tumor growth and metastasis

and is a promising target for cancer therapy [35,36]. Monitoring microvascular density and branching patterns is an indispensable tool for evaluation and development of anti-angiogenic drugs. A solid tumor with a diameter  $>1 \text{ mm}$  requires an adequate blood supply for growth and metastasis [1,2]. Therefore, it is critical for early detection and early therapy of tumor to have an effective method to *in situ* monitor the tumor angiogenesis in a noninvasive way. As illustrated above, PEGylated  $\text{Ag}_2\text{S}$  QDs offer maximum tissue penetration depth, high spatial and temporal resolution, as well as appreciable blood circulation half-time, which facilitate the *in vivo* real-time imaging of tumor-induced angiogenesis. To trace tumor angiogenesis dynamics *in vivo*, intravital fluorescence images were acquired 30 min post-injection of PEGylated  $\text{Ag}_2\text{S}$  QDs (1 mg/mL, 200  $\mu\text{L}$ ) into the tail vein of female athymic nude mice on day 5, 8, 15 and 21 after 4T1 tumor transplantation, respectively. Fig. 4 showed the formation of new blood vessels induced by the 4T1 mammary tumor. An increase in the fluorescence signal was observed in the early tumor stages, which was mainly distributed at the periphery of the tumor (Fig. 4a). Vascular structures were recruited to feed the tumor which was clearly identified on the 15th day after the subcutaneous tumor xenograft (Fig. 4a). With continuous growth of the 4T1 tumor, abundant irregularly branching blood vessels were formed and were surrounding the

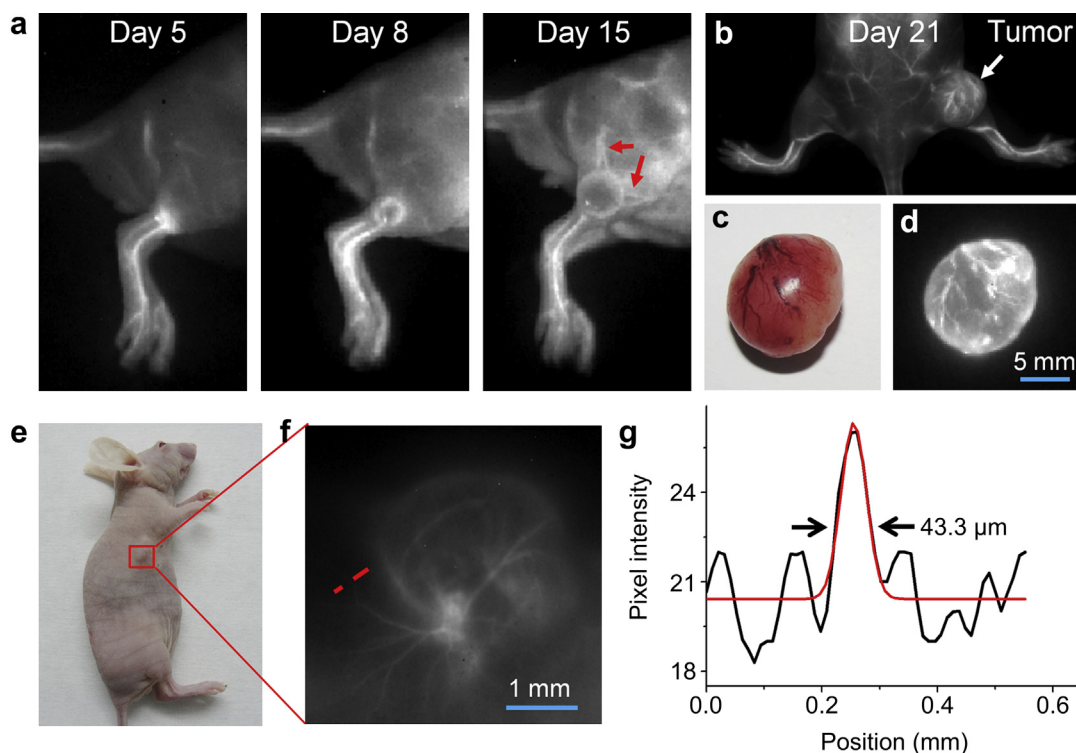


**Fig. 4.** *In vivo* real-time visualization of tumor-induced angiogenesis. NIR-II fluorescence images of the 4T1 mammary tumor-bearing mouse. Fluorescence images were acquired after 30 min post tail vein injection of PEGylated  $\text{Ag}_2\text{S}$  QDs (1 mg/mL, 200  $\mu\text{L}$ ) on day 5, 8, 15 (a) and 21 (b) after 4T1 tumor transplantation, respectively. Red arrow unambiguously visualized the tumor-induced angiogenesis *in vivo* with the help of NIR-II PEGylated  $\text{Ag}_2\text{S}$  QDs, whereas the white arrow located the 4T1 tumor. (c) Daylight image of the tumor extracted from the mouse. (d) NIR-II fluorescence image of the tumor. (e) Color photo of U87MG tumor-bearing mouse. (f) Amplified fluorescent image of the selected region in (e). (g) A cross-sectional intensity profile measured along the red-dashed line in (f) with its peak fitted to Gaussian functions. (For interpretation of the references to color in this figure legend, the reader is referred to the web version of this article.)

tumor, showing typical characteristics of tumor blood vessels (Fig. 4b). Accumulation of blood vessels in the tumor tissue was further confirmed by anatomic observation (Fig. 4c and d). The results showed a strong correlation between the NIR-II fluorescence signal of the  $\text{Ag}_2\text{S}$  QDs and the blood vessel density in the

tumor area in our model. Furthermore, with the help of a zoom-in lens, the angiogenesis of a much smaller human glioblastoma (U87MG) ( $\sim 2.7$  mm in diameter) was clearly observed *in vivo* using  $\text{Ag}_2\text{S}$  QDs (Fig. 4e and f). As shown in Fig. 4g, the cross-sectional analysis of a tumor blood vessel gives the diameter of  $\sim 43$   $\mu\text{m}$ .

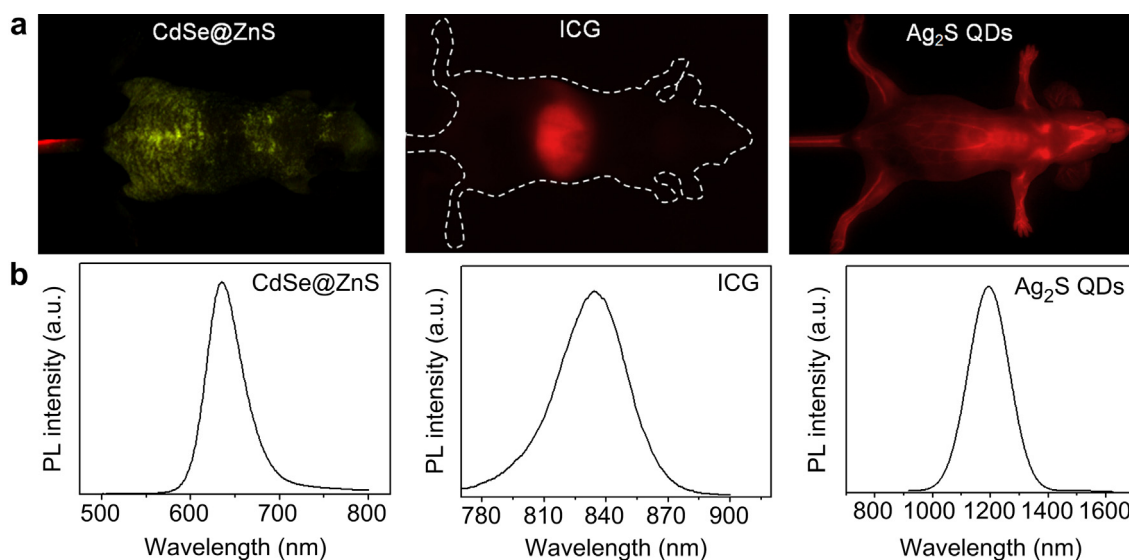


**Fig. 5.** *In vivo* fluorescence images of CdSe@ZnS QDs, ICG (NIR-I), and  $\text{Ag}_2\text{S}$  QDs (NIR-II) in nude mice. (a) CdSe@ZnS QDs, ICG and  $\text{Ag}_2\text{S}$  QDs were injected intravenously into mice and fluorescence images were taken after i.v. injection for 5 min under excitation at 455, 704, and 808 nm, respectively. The green-yellow signal of the mouse injected with CdSe@ZnS QDs indicates the strong autofluorescence of tissues in the visible emission window. The red signal concentrated in the liver of the mouse injected with ICG indicates the short blood circulation half-time. The red signal widely distributed in the whole body of mouse injected with  $\text{Ag}_2\text{S}$  QDs indicates the long blood circulation half-time. (b) The PL spectra of CdSe@ZnS QDs, ICG and  $\text{Ag}_2\text{S}$  QDs. (For interpretation of the references to color in this figure legend, the reader is referred to the web version of this article.)

These observations are encouraging for the future clinical application of Ag<sub>2</sub>S QDs in the early detection and therapy of tumor.

We successfully demonstrated that NIR-II Ag<sub>2</sub>S QDs can be used for *in vivo* real-time visualization of circulatory systems and tumor angiogenesis, because of less autofluorescence, deeper tissue penetration, higher spatial and temporal resolution in the NIR-II window in comparison to the visible emission CdSe@ZnS QDs (emission peak at 635 nm) and NIR-I ICG (emission peak at 835 nm) (Fig. 5). These interesting results may be of high significance for the following future clinical applications. (1) Intraoperative guidance for SLN identification and dissection. In comparison with the previously reported CdTe/CdSe QDs with emission peak at 850 nm using for SLN mapping [10], NIR-II Ag<sub>2</sub>S QDs with lower tissue phantom and deeper tissue penetration (Fig. 5 and Supplementary Fig. S3) allow acquisition of higher-resolution images of deep structures, and more accurate image guidance for SLN dissection will be available with the help of NIR-II imaging. (2) Assessment of blood supply in tissues and organs. Transplanted tissues or organs must be connected to the recipient's blood vessels in order to restore normal blood supply and for the transplant to succeed. Fluorescence imaging with NIR-II Ag<sub>2</sub>S QDs has potential as a new method for rapid assessment of the blood supply in tissues and organs after transplantation. Unlike CT, MR perfusion imaging of blood flow, which need continuous injection of high dose of contrast agent, PEGylated Ag<sub>2</sub>S QDs, possessing an optimal blood circulation half-time of ~4.1 h, remain highly fluorescent in the blood flow for more than 9 h (Fig. S8), which benefits the direct observation and assessment of vascular structure and hemodynamics of the transplanted tissues and organs. (3) Screening and evaluation of anti-angiogenic drugs. Tumor growth is prevented when angiogenesis is inhibited. Our *in vivo* NIR-II imaging technique can provide a noninvasive method for screening and evaluating anti-angiogenic drug, avoiding the requirement of tissue specimens in conventional antibody-based histological methods. It is worth noting that our previous results have demonstrated the decent biocompatibility of Ag<sub>2</sub>S QDs, in terms of cytotoxicity, blood biochemistry, hematological analysis, and histological examinations [31,33]. For their preclinical applications, more detailed toxicology investigations on Ag<sub>2</sub>S QDs, such as genotoxicity and reproductive toxicity, are underway.

#### 4. Conclusion

In summary, our results clearly show that NIR-II Ag<sub>2</sub>S QDs enable noninvasive and dynamic visualization of the circulatory system, including lymphatic drainage, vascular networks, and angiogenesis and may play an important role in diagnosis and therapy of circulatory system-related diseases. Maximum penetration depth with high feature fidelity indicates that NIR-II Ag<sub>2</sub>S QDs will provide great opportunities for future clinical applications, well beyond traditional static NIR-I techniques and immunohistochemical methods.

#### Conflicts of interest

No financial conflict of interest was reported by the authors of this paper.

#### Acknowledgments

This work was financially supported by CAS Bairen Ji Hua Program and Strategic Priority Research Program (No. XDA01030200), MOST (No. 2011CB965004), NSFC (No. 21073225), NSF Jiangsu Province (BK2012007) and CAS/SAFEA International Partnership Program for Creative Research Teams.

#### Appendix A. Supplementary data

Supplementary data related to this article can be found at <http://dx.doi.org/10.1016/j.biomaterials.2013.10.010>.

#### References

- [1] Folkman J, Bach M, Rowe JW, Davidoff F, Lambert P, Hirsch C, et al. Tumor angiogenesis: therapeutic implications. *N Engl J Med* 1971;285:1182–6.
- [2] Folkman J. What is the evidence that tumors are angiogenesis dependent. *J Natl Cancer Inst* 1990;82:4–6.
- [3] Tsien RY. Imaging imaging's future. *Nat Rev Mol Cell Biol* 2003;(Suppl.):S516–21.
- [4] Mariani G, Moresco L, Viale G, Villa G, Bagnasco M, Canavese G, et al. Radio-guided sentinel lymph node biopsy in breast cancer surgery. *J Nucl Med* 2001;42:1198–215.
- [5] Mariani G, Gipponi M, Moresco L, Villa G, Bartolomei M, Mazzarol G, et al. Radioguided sentinel lymph node biopsy in malignant cutaneous melanoma. *J Nucl Med* 2002;43:811–27.
- [6] O'Leary DH, Polak JF, Kronmal RA, Manolio TA, Burke GL, Wolfson SK, et al. Carotid-artery intima and media thickness as a risk factor for myocardial infarction and stroke in older adults. *N Engl J Med* 1999;340:14–22.
- [7] Rizzo V, Steinfeld R, Kyriakides C, Defouw DO. The microvascular unit of the 6-day chick chorioallantoic membrane: a fluorescent confocal microscopic and ultrastructural morphometric analysis of endothelial permselectivity. *Microvasc Res* 1993;46:320–32.
- [8] Jilani SM, Murphy TJ, Thai SNM, Eichmann A, Alva JA, Iruela-Arispe ML. Selective binding of lectins to embryonic chicken vasculature. *J Histochem Cytochem* 2003;51:597–604.
- [9] Pardanaud L, Altmann C, Kitos P, Dieterlenlievre F, Buck CA. Vasculogenesis in the early quail blastodisc as studied with a monoclonal-antibody recognizing endothelial-cells. *Development* 1987;100:339–49.
- [10] Kim S, Lim YT, Soltesz EG, De Grand AM, Lee J, Nakayama A, et al. Near-infrared fluorescent type II quantum dots for sentinel lymph node mapping. *Nat Biotechnol* 2004;22:93–7.
- [11] Larson DR, Zipfel WR, Williams RM, Clark SW, Bruchez MP, Wise FW, et al. Water-soluble quantum dots for multiphoton fluorescence imaging *in vivo*. *Science* 2003;300:1434–6.
- [12] Smith AM, Mancini MC, Nie SM. Bioimaging second window for *in vivo* imaging. *Nat Nanotechnol* 2009;4:710–1.
- [13] Welsher K, Sherlock SP, Dai HJ. Deep-tissue anatomical imaging of mice using carbon nanotube fluorophores in the second near-infrared window. *Proc Natl Acad Sci U S A* 2011;108:8943–8.
- [14] Lim YT, Kim S, Nakayama A, Stott NE, Bawendi MG, Frangioni JV. Selection of quantum dot wavelengths for biomedical assays and imaging. *Mol Imaging* 2003;2:50–64.
- [15] Won N, Jeong S, Kim K, Kwag J, Park J, Kim SG, et al. Imaging depths of near-infrared quantum dots in first and second optical windows. *Mol Imaging* 2012;11:338–52.
- [16] Liu Z, Cai WB, He LN, Nakayama N, Chen K, Sun XM, et al. *In vivo* biodistribution and highly efficient tumour targeting of carbon nanotubes in mice. *Nat Nanotechnol* 2007;2:47–52.
- [17] Liu Z, Tabakman S, Welsher K, Dai HJ. Carbon nanotubes in biology and medicine: *in vitro* and *in vivo* detection, imaging and drug delivery. *Nano Res* 2009;2:85–120.
- [18] Welsher K, Liu Z, Sherlock SP, Robinson JT, Chen Z, Daranciang D, et al. A route to brightly fluorescent carbon nanotubes for near-infrared imaging in mice. *Nat Nanotechnol* 2009;4:773–80.
- [19] Robinson JT, Welsher K, Tabakman SM, Sherlock SP, Wang HL, Luong R, et al. High performance *in vivo* near-IR (>1 μm) imaging and photothermal cancer therapy with carbon nanotubes. *Nano Res* 2010;3:779–93.
- [20] Hong GS, Tabakman SM, Welsher K, Chen Z, Robinson JT, Wang HL, et al. Near-infrared-fluorescence-enhanced molecular imaging of live cells on gold substrates. *Angew Chem Int Edit* 2011;50:4644–8.
- [21] Robinson JT, Hong G, Liang Y, Zhang B, Yaghi OK, Dai H. *In vivo* fluorescence imaging in the second near-infrared window with long circulating carbon nanotubes capable of ultrahigh tumor uptake. *J Am Chem Soc* 2012;134:10664–9.
- [22] Hong GS, Lee JC, Robinson JT, Raaz U, Xie LM, Huang NF, et al. Multifunctional *in vivo* vascular imaging using near-infrared II fluorescence. *Nat Med* 2012;18:1841.
- [23] Antaris AL, Robinson JT, Yaghi OK, Hong GS, Diao S, Luong R, et al. Ultra-low doses of chirality sorted (6,5) carbon nanotubes for simultaneous tumor imaging and photothermal therapy. *Acs Nano* 2013;7:3644–52.
- [24] Yi HJ, Ghosh D, Ham MH, Qi JF, Barone PW, Strano MS, et al. M13 phage-functionalized single-walled carbon nanotubes as nanoprobes for second near-infrared window fluorescence imaging of targeted tumors. *Nano Lett* 2012;12:1176–83.
- [25] Choi HS, Liu W, Misra P, Tanaka E, Zimmer JP, Ipe BI, et al. Renal clearance of quantum dots. *Nat Biotechnol* 2007;25:1165–70.
- [26] Harrison MT, Kershaw SV, Burt MG, Eychmuller A, Weller H, Rogach AL. Wet chemical synthesis and spectroscopic study of CdHgTe nanocrystals with strong near-infrared luminescence. *Mat Sci Eng B-Solid* 2000;69:355–60.

- [27] Wehrenberg BL, Wang CJ, Guyot-Sionnest P. Interband and intraband optical studies of PbSe colloidal quantum dots. *J Phys Chem B* 2002;106:10634–40.
- [28] Bakueva L, Gorelikov I, Musikhin S, Zhao XS, Sargent EH, Kumacheva E. PbS quantum dots with stable efficient luminescence in the near-IR spectral range. *Adv Mater* 2004;16:926–9.
- [29] Du YP, Xu B, Fu T, Cai M, Li F, Zhang Y, et al. Near-infrared photoluminescent Ag<sub>2</sub>S quantum dots from a single source precursor. *J Am Chem Soc* 2010;132:1470–1.
- [30] Shen SL, Zhang YJ, Peng L, Du YP, Wang QB. Matchstick-shaped Ag<sub>2</sub>S-ZnS heteronanostructures preserving both UV/blue and near-infrared photoluminescence. *Angew Chem Int Edit* 2011;50:7115–8.
- [31] Zhang Y, Hong GS, Zhang YJ, Chen GC, Li F, Dai HJ, et al. Ag<sub>2</sub>S quantum dot: a bright and biocompatible fluorescent nanoprobe in the second near-infrared window. *ACS Nano* 2012;6:3695–702.
- [32] Hong GS, Robinson JT, Zhang YJ, Diao S, Antaris AL, Wang QB, et al. In vivo fluorescence imaging with Ag<sub>2</sub>S quantum dots in the second near-infrared region. *Angew Chem Int Edit* 2012;51:9818–21.
- [33] Zhang Y, Zhang YJ, Hong GS, He W, Zhou K, Yang K, et al. Biodistribution, pharmacokinetics and toxicology of Ag<sub>2</sub>S near-infrared quantum dots in mice. *Biomaterials* 2013;34:3639–46.
- [34] Hillman EMC, Moore A. All-optical anatomical co-registration for molecular imaging of small animals using dynamic contrast. *Nat Photonics* 2007;1:526–30.
- [35] Jain RK. Normalization of tumor vasculature: an emerging concept in anti-angiogenic therapy. *Science* 2005;307:58–62.
- [36] Brindle K. New approaches for imaging tumour responses to treatment. *Nat Rev Cancer* 2008;8:94–107.